Innovation and Optimization of Aeration in Free Bubbling Flat Sheet MBRs

Bing Wang[a,b], Yan Zhang[a], Guixiao Zhang[a], Kaisong Zhang[b*], Robert W. Field[c,d]

[a] *College of Environmental Science and Engineering/Sino-Canada Joint R&D Centre for Water and Environmental Safety, Nankai University, Tianjin 300071, PR China*

[b] *Key Laboratory of Urban Pollutant Conversion, Institute of Urban Environment, Chinese Academy of Sciences, Xiamen 361021, China*

[c] *Faculty of Engineering and Environment, Northumbria University, Newcastle NE1 8ST, UK*

[d] *Department of Engineering Science, University of Oxford, Oxford OX1 3PJ, UK*

Published in Journal of Membrane Science

DOI 10.1016/j.memsci.2021.119522

Abstract

Free bubbling in flat sheet MBRs has been widely used in water treatment to control membrane fouling, however, the associated aeration cost discourages its wider application. To counter this drawback an innovative design of the aeration system is proposed and its evaluation indicates significantly high potential. The guiding aim is the establishment of sufficient shear stress in all membrane channels at an economical specific air demand (SAD_m). Based upon a validated Computational Fluid Dynamics (CFD) study, hydrodynamic features including shear stress, bubble size and the distribution of bubbles across neighboring channels were predicted for two designs. For both a mini 100-sheets commercial FSMBR (size of plates 448mm×245mm) and a full-scale standard unit with 1800mm×490mm plates, it was shown that sufficient hydrodynamic effect is induced with our modified free aeration design in a manner that moves beyond seeking to achieve bland uniformity between channels. The optimal configuration featured a channel gap at 5 mm and an aerator with an additional large side nozzle operating at an inlet velocity of 2.6 m/s. Such an arrangement would cover 12 channels. Through optimization the air consumption was successfully reduced giving a SAD_m of 0.28 $Nm^3m^{-2}h^{-1}$, corresponding to 46% reduction with respect to traditional industrial usage of 0.51 $Nm^3m^{-2}h^{-1}$.

Key Words

Flat sheet MBR; free bubbling; CFD; fouling control; economical air consumption.

1. Introduction

Membrane bioreactors are an established technology widely used in water treatment [1-3]. Aeration is applied to induce gas-liquid two-phase turbulence to ameliorate membrane fouling [4-7]. The flat sheet MBR (FSMBR), one of the two major configurations of MBRs, was first introduced by the Kubota corporation. Today's FSMBRs with their various aeration methods provide technically effective strategies to affect sufficient fouling amelioration at a moderate air consumption [8-11]. Nevertheless this air consumption is the major operating cost [12, 13] which can be seen as excessively high. Herein an innovative design, which gives sufficient shear stress at a reduced specific air demand (SAD_m), is introduced.

According to the flow pattern in the FSMBR, the aeration processes can be generally classified as either free bubbling or intermittent bubbling. A number of numerical and experimental work have been developed for these two bubbling regimes, in order to analyze and compare of the induced shear stress and optimize the hydrodynamics for fouling control [14-17]. However, their conclusions were based on observations for small modules consisting of two pieces of 0.1 m^2 flat sheet membranes. Such units are far removed in scale from operational FSMBR where the size of the membrane panels and their number are much greater (i.e. > 100 sheets). Hence there is a research gap and some further comprehensive work on how to induce sufficiently intense hydrodynamic effects within full-scale FSMBRs as used for industrial application.

For full-scale commercial MBR, where the possibility of making experimental measurements and observations is highly limited, the CFD (Computational Fluid Dynamics) is a very useful tool [18, 19] to explore the hydrodynamics of gas induced flow

in MBRs. There are several multi-phase simulation methods for gas-liquid interface calculations, such as Euler-Euler, mixture and VOF (Volume of Fluid) methods. The VOF is generally applied as it is a more suitable method by which to compute the motion of bubbles in a liquid. This is achieved through incorporating an additional volume fraction equation, which is detailed below in section 2.2.2. Liu et al. [20] optimized the membrane module design and operation parameters for full-scale HF MBR through CFD simulation and RTD experiments. Radaei et al. [21] simplified and calibrated for high-packed HF membrane module, reported the asynchronous bubble release induced more evenly distributed shear. Zhang and Wei et al. [16, 22-24] summarized its practical application in FSMBR system, which improved shear stress but reduce energy consumption. Wu et al. [25] explored the membrane unit location in the large amount water treatment application to optimize the hydrodynamics of plenty units of MBR. Liu et al. [26] proposed aeration of bent-sheet system to reduce the uneven slug bubble distribution.

Unfortunately, limited research concerning some of the problems faced in application of the bubbling process in FSMBR industry has taken place. Questions remaining include how to provide sufficient shear stress onto every membrane plate at full-scale application. In our previous work on the minimization of inhomogeneity in shear stress distribution among membrane wall surfaces, a novel intermittent aeration method was constructed [27]. It was shown that through a two-stage bubble development process (coalescence and split) one could achieve coverage throughout a large-scale commercial FSMBR.

More recently we have advocated and advanced a novel intermittent bubbling process with large-coalescence bubbles, which has advantages over those aerations without coalescence [28]. Subsequent research refined the aeration process and set optimal

conditions such as air flow rate, channel gap and thickness of membrane so as to achieve a uniform slug bubble distribution with high average shear stress [29]. With the increase of the number of super large MBR (≥100,000 m^3/d), the two decks FSMBR system, which has a higher capacity of water treatment is the focus in industry. Hence, three-stage intermittent bubbling process (bubble coalescence-split-reunion) in a double-deck FSMBR configuration was studied therein to provide sufficient shear stress onto all membranes whilst economically decreasing the air consumption [30]. The process has been applied commercially by Oxiamembrane Co. Ltd (http://www.oxiamem.com).

However where space in general and headroom in particular is limited this approach is impractical. For example where mini FSMBR devices are deployed (e.g. water reclamation and 'black' water reuse) free bubbly flow would still be the preferred choice. Indeed, the free bubbling regime remains popular in large-scale industry. In spite of this preference there is limited research about how to control this bubbly aeration process for (a) a group of membrane panels and (b) different scales, such as mini type and full-scale FSMBR. In practice, how to decrease the air consumption of the free bubbling process in order to save energy whilst still guaranteeing control of fouling whilst changing scale is still a significant unresolved problem. This is addressed herein concurrent with the introduction and evaluation of an innovative aerator.

In order to address these problems, based on our previous study results, CFD simulation is used to evaluate an innovative design of aerator for the free bubbling process. The motivation for investigating an open-end aerator is two-fold, firstly it is to enhance the bubbly flow hydrodynamic effect whilst simultaneous seeking to reduce air consumption, which dominates operating costs and is a key factor in determining the industrial adoption

or otherwise of MBRs. A secondary reason for adding a side nozzle (the top opening apertures are retained) is that an open end allows any sediment inside an aerator to be discharged.

In the current work, two configurations of aerator design were compared for the entire free bubbling process, including bubble development and induced shear stress. The two types were the conventional design and our innovative design with the additional end nozzle (the top opening apertures are retained). Combination of two critical parameters were investigated through CFD simulations using the model validated in our previous work [27]. The influence of channel gap and air flow rate upon bubble features and shear stress were studied, including the distribution between channels which can be tailored to optimize beneficial liquid circulation. The modified aerator design was not only studied for mini type FSMBR with 488 mm high plates, it was also applied to a full-scale FSMBR with a membrane height of 1800 mm. In addition to studying the influence of operating parameters on shear stress great attention was paid to the specific air demand (SAD_m) because the air consumption in FSMBRs has often been considered to be excessive. Herein the standardized measure, SAD_m, the rate of air usage per unit of membrane area was evaluated for the new innovative design and compared to typical values, which expressed in units of Nm^3h^{-1} per m^2 (or the equivalent $Nm^3m^{-2}h^{-1}$.)

2. Methods

2.1 Experimental study

The free bubbling behavior in this large-scale FSMBR were investigated by both CFD and experimental studies. The schematic diagram of experiment is shown in Fig. 1, the tank

dimensions were 600×400×1200 mm (L×T×H). Bubbly flow was generated, and its development could be observed.

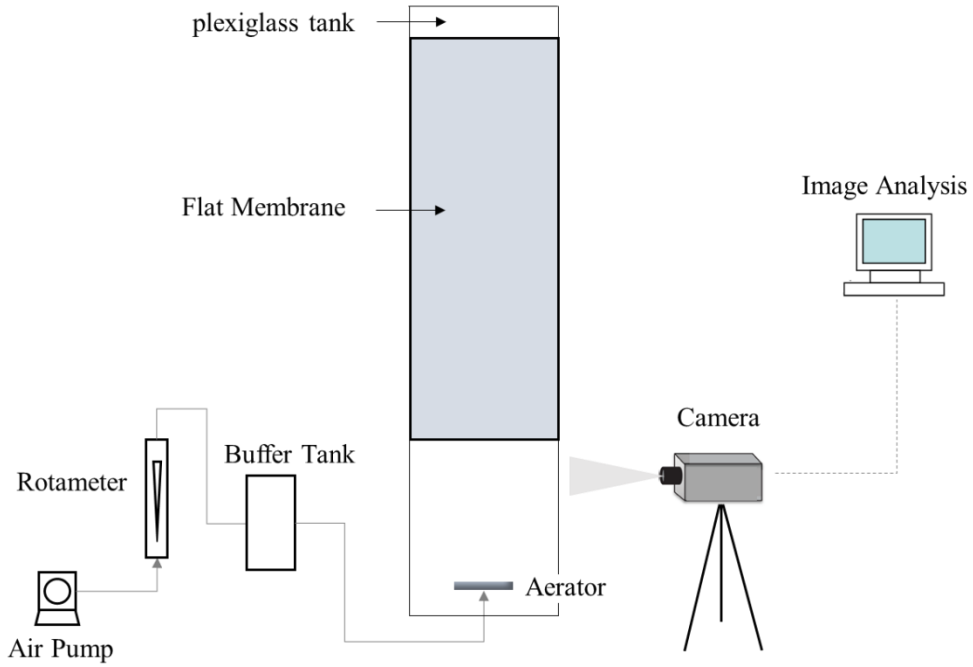

Fig. 1 Free bubbling hydrodynamics experimental rig.

The aerator was of O.D. 20 mm with 4 apertures of O.D. 4 mm. Two configurations of aerators design, conventional with a close end and with an additional large nozzle (i.e. the open end) are shown in Fig. 2. There are four small apertures on the top of aerator in both designs, but there is an additional large opening in the current modified configuration.

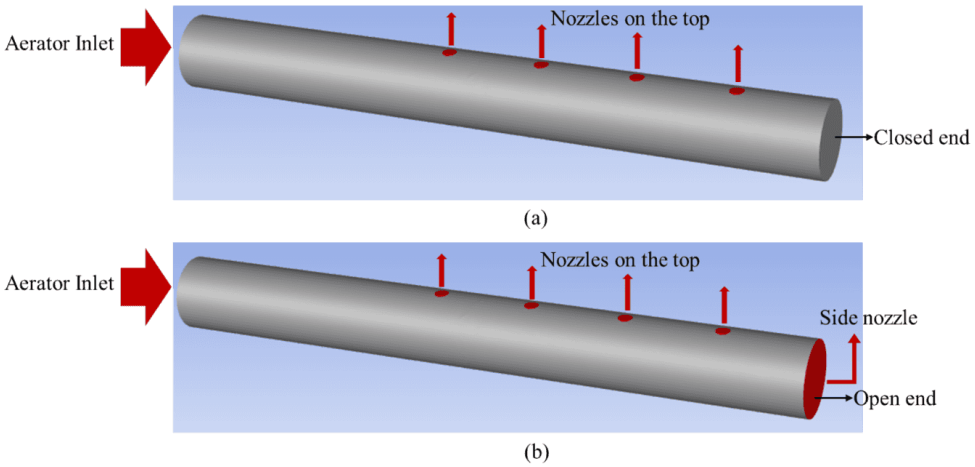

Fig. 2 Two types of aerator configurations with the same four small apertures on the top: (a) Configuration 1: close end with no side nozzle; (b) Configuration 2: open end with a large side nozzle.

As shown in Fig. 1, air passed through the air flow rotameter and was directed to the tank. Bubbling was assessed at five air velocities from 1 m/s to 3.7 m/s. Bubble behavior was observed by a video camera placed in the front for visual recording. A CMOS camera was used with 1024×1024-pixel high speed (FASTCAM SA1.1, Photron, Japan) equipped with a Nikon Micro 60 mm F2.8D lens up at 480 fps. A MATLAB program was run to process the images and obtain quantitative information on bubble characteristics. The number of bubbles from each nozzle was divided by the time interval of 1 min to obtain the bubble frequency. Bubble size was measured through the Image J software. Experiments were conducted three times at room temperature.

2.2 CFD simulation

2.2.1 Physical model and meshing

The dimensions of membrane panels were 245×6×488 mm (L×T×H) and 490×6×1800 mm (L×T×H) for mini type and full-scale FSMBRs respectively, these being the dimensions of those supplied by Oxiamembrane Co., Ltd, China. The diameter of aerator was 20 mm and it was fixed 350 mm below the stack of membrane plates.

To simulate this free bubbling process, the 3D computational geometry was built and meshed in GAMBIT 2.4.6. High-quality mesh of Cooper-type hex was used to divide the computing domain. The total number of membrane plates (Oxiamembrane Co., Ltd, China) used in this simulation covered 12 plates, but because of a symmetric boundary condition one only needs to simulate 6; this saves computational time. To control the hydrodynamic features of fine bubbles in the channel between every pair of membrane plate, simulation was operated under different air flow velocity from the aerator inlet and channel gap. The spacing between two adjacent membrane sheets was varied from 3.5 mm to 7 mm in accord with industrial application requirements. Additionally, the height of membrane was enlarged to be 1800 mm, in order to determine in full-scale FSMBR with sufficient hydrodynamic effect of shear stress. Hence, a series of computational geometries with different channel gaps were set up. The typical mesh was shown in Fig. 3, the highest average EquiSize Skew parameter was 0.658 for the entire computation domain, which indicated high mesh quality. Table 1 showed detailed mesh information for different computational geometries.

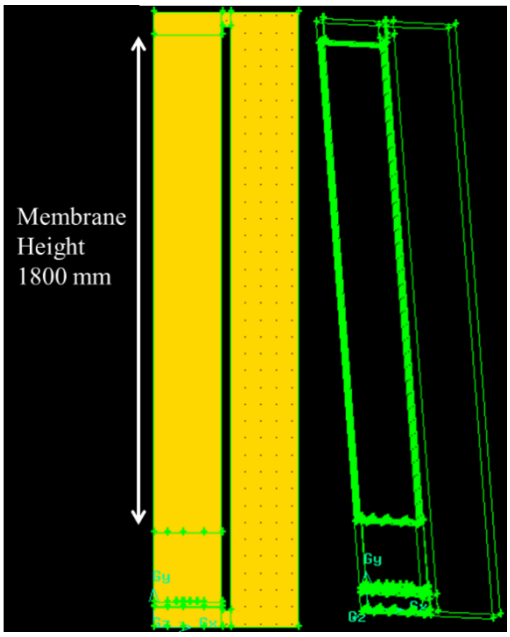

(a)

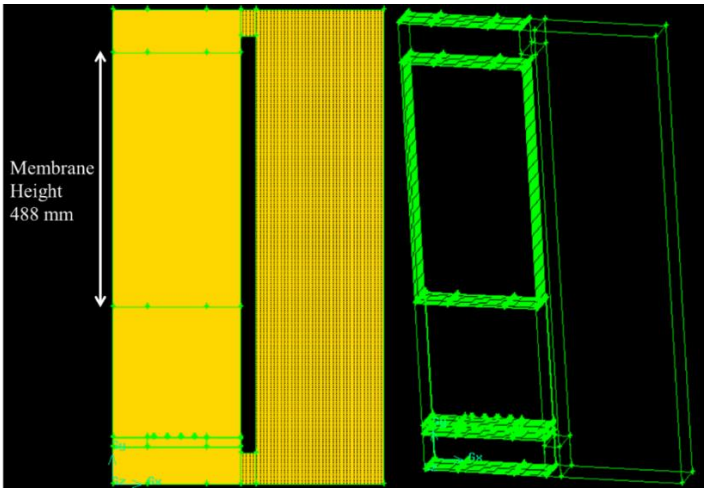

(b)

Fig. 3 Mesh structure of computational domain for free bubbling regime in (a) full-scale and (b) mini FSMBR systems generated by GAMBIT software.

Table 1 Mesh information for various 3D computational geometries

Aerator with closed end (CE) and open end (OE) in mini FSMBR system

Name	Height of Membrane Plate (mm)	Width of Channel (mm)	Number of Cells	Number of Faces	Number of Nodes
CE-C5	488	5	1,477,176	4,584,271	1,745,090
OE-C3.5	488	3.5	1,598,856	5,082,426	1,939,282
OE-C4.5	488	4.5	1,484,008	4,772,466	1,860,256
OE-C5	488	5	1,448,483	4,645,937	1,816,706
OE-C6	488	6	1,404,208	4,529,141	1,776,506
OE-C7	488	7	1,362,712	4,402,612	1,732,956

Aerator with open end in normal FSMBR system

Name	Height of Membrane Plate (mm)	Width of Channel (mm)	Number of Cells	Number of Faces	Number of Nodes
OE-C5-H1800	1800	5	2,192,095	7,043,651	2,661,083

2.2.2 Governing equations

3D simulations were conducted with ANSYS FLUENT 14.5. The fine bubbles coalescence, deformation, collision and breaking process were calculated by three-dimensional gas-liquid two-phase flow simulation method. VOF (Volume of Fluid) model combined with CSF (continuum surface force) model was used to track gas-liquid interface

[31, 32]. The details of mass and momentum conservation equations and additional governing equations for turbulence and interface tracking related in the simulation for incompressible two-phase flow are given as following. The mass and momentum conservation equations can be expressed as

$$\frac{\partial \rho}{\partial t} + \nabla(\rho \vec{u}) = 0 \tag{1}$$

$$\frac{\partial}{\partial t}(\rho \vec{u}) + \nabla(\rho \vec{u}\vec{u}) = -\nabla P + \rho \vec{g} + \rho \vec{F} + \nabla \vec{\tau} \tag{2}$$

where the right three items in Eqn. (2) are the pressure, gravitational acceleration, and external force, respectively. In each control volume, the properties of density ρ and dynamic viscosity μ were determined by volume-fraction-averaged method for an n-phase system:

$$\rho = \sum \alpha_q \rho_q \tag{3}$$

$$\mu = \sum \alpha_q \mu_q \tag{4}$$

Where,

$$\sum_{q=1}^{n} \alpha_q = 1 \tag{5}$$

Turbulence induced from aeration could be calculated through the realizable *k–ε* model by Shih et al. [33]. It has the substantial improvements over the standard k–ε model not only for the flow features including strong streamline curvature, vortices, and rotation; but for flows with complex secondary flow features as well, which were primarily flow features in the free bubbling process of this work. The modeled transport equations for *k* (turbulence kinetic energy) and *ε* (dissipation rate) in the realizable *k–ε* model are shown as Eqs. (6) and (7), respectively:

$$\frac{\partial}{\partial t}(\rho k) + \frac{\partial}{\partial x_j}(\rho k u_j) = \frac{\partial}{\partial x_j}\left[\left(\mu + \frac{\mu_t}{\sigma_k}\right)\frac{\partial k}{\partial x_j}\right] + G_k + G_b - \rho\varepsilon - Y_M \quad (6)$$

$$\frac{\partial}{\partial t}(\rho\varepsilon) + \frac{\partial}{\partial x_j}(\rho\varepsilon u_j) = \frac{\partial}{\partial x_j}\left[\left(\mu + \frac{\mu_t}{\sigma_\varepsilon}\right)\frac{\partial \varepsilon}{\partial x_j}\right] + \rho C_1 S\varepsilon - \rho C_2 \frac{\varepsilon^2}{k + \sqrt{\upsilon\varepsilon}} + C_{1\varepsilon}\frac{\varepsilon}{k}C_{3\varepsilon}G_b + S_\varepsilon \quad (7)$$

Where

$$\mu_t = \rho C_\mu \frac{k^2}{\varepsilon}$$

$$C_1 = \max\left[0.43, \frac{\eta}{\eta + 5}\right]$$

$$\eta = S\frac{k}{\varepsilon}$$

$$S = \sqrt{2S_{ij}S_{ij}}$$

The term G_k, represents the production of turbulence kinetic energy as defined:

$$G_k = -\rho\overline{u_\iota' u_j'}\frac{\partial u_j}{\partial x_i}$$

The *k*–*ε* model accounts for the generation of k due to buoyancy by G_b and its corresponding contribution to the production of ε, which is given by

$$G_b = \beta g_i \frac{\mu_t}{Pr_t}\frac{\partial T}{\partial x_i}$$

Y_M represents dilatation dissipation from turbulence of compressibility effect, which is normally neglected in the incompressible flows. Instead of constant, C_μ is a function of rotation rates, mean strain and the turbulence fields. C_2 and $C_{1\varepsilon}$ are constants. Turbulent Prandtl numbers of k and ε are represented by σ_k and σ_ε, respectively.

The Continuum Surface Force (CSF) model by Brackbill et al. [32] indicated that surface tension was continuous three-dimensional effect across an interface between two phases, rather than a boundary value condition on the interface. It is modeled in terms of pressure jump and calculated through a source term in momentum, which is shown as:

$$p_L - p_G = \sigma\kappa \tag{8}$$

$$\underset{F\ vol}{\rightarrow} = \sigma \frac{2\rho\kappa\nabla_{\alpha_G}}{(\rho_L + \rho_G)} \tag{9}$$

where the curvature κ is defined with divergence of the unit normal, $\hat{n}$:

$$\kappa = \nabla\hat{n}$$

$$\hat{n} = \frac{n}{|n|}, n = \nabla\alpha_q$$

2.2.3 Numerical methods and boundary conditions

The simulations were proceeded through the pressure-based solver. Momentum equations and k–ε turbulence was discretized by second order upwind scheme, and pressure-velocity coupling was solved by PISO. The volume fraction function is solved using the geometric reconstruction scheme based on piecewise linear interface calculation (PLIC). Aerator air velocity was ranged between 1 m/s and 3.7 m/s, whilst liquid phase velocity was set to be zero. Stationary boundary conditions were used for all of the walls with a condition of no fluid-slip at the membrane wall surfaces.

3. Results and Discussion

3.1 Model qualification

The model has been validated by experimental measurement as detailed here. The bubble column height from the apertures were measured for both modified and traditional aerators. Using both experimental data and CFD simulation results, the bubble features

were qualitatively and quantitatively compared - see Table 2, Table 3 and Figure 4. For the novel open-end aeration design, the bubble size was observed at five different air flow rates between 1 m/s to 3.7 m/s. Experimental data showed that the bubble dimension of the top apertures varied from 28 mm to 49 mm, and for the side nozzle from 40 mm to 84 mm. For low velocity range of 1 m/s to 2 m/s, the side nozzle bubble was around 50 mm, but it increased to be around 80 mm as the velocity increased to more than 2.6 m/s. The bubble frequency varied from 4 s^{-1} to 16 s^{-1} for the top and side nozzles, as the aeration velocity increased from 1 m/s to 3.7 m/s, which agreed with CFD results.

The bubble size and bubble frequency of the new design were also compared with that of the traditional design. For the traditional design, which only has top apertures, the air column height was around 50 mm and the bubble frequency was 11 s^{-1} for all 4 apertures. The modified design with an open-end gave similar results for its top apertures but additionally the end nozzle produced large bubbles with height of 84 mm and bubble frequency of 9 s^{-1}. (The actual values for the air column height and bubble frequency of the top apertures were 47 mm and 10 s^{-1} respectively.)

Table 2 Bubble column height comparison between CFD results and experimental data

Bubble column height (mm) of data Innovative aerator design with open end (OE) and 5 mm channel gap				
Inlet air Velocity (m/s)	Top Aperture experimental	Top Aperture simulation	Side nozzle experimental	Side nozzle simulation
1	28±2	30	40±1	39
2	37±1	38	55±2	56

2.6	47±2	46	84±3	82
3	49±3	47	80±2	78
3.7	47±2	45	78±2	76
Traditional aerator design with closed end (CE) and 5 mm channel gap				
2.6	52±2	50	0	0

Table 3 Bubble rising frequency comparison between CFD results and experimental data

Bubble rising frequency (s^{-1}) of data				
Innovative aerator design with open end (OE) and 5 mm channel gap				
Inlet air Velocity (m/s)	Top Aperture experimental	Top Aperture simulation	Side nozzle experimental	Side nozzle simulation
1	4±1	5	3±1	4
2	8±1	6	6±2	9
2.6	10±2	11	9±1	7
3	13±1	10	10±2	11
3.7	16±2	14	12±1	13
Traditional aerator design with closed end (CE) and 5 mm channel gap				
2.6	11±1	10	0	0

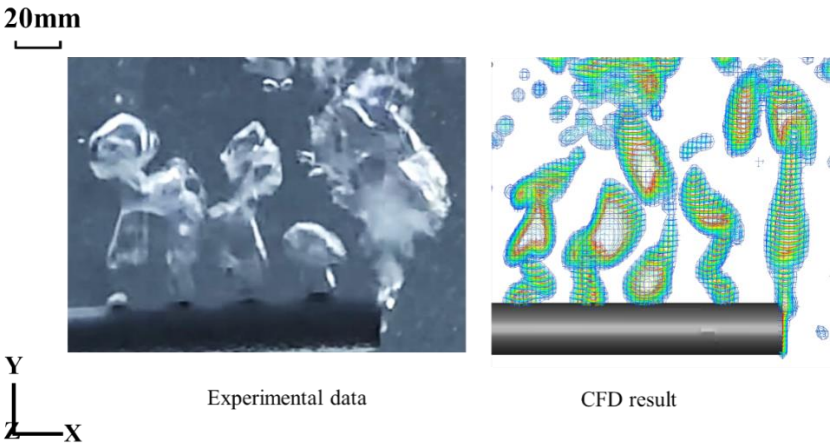

Fig. 4 Comparison of experimental data and CFD results for bubble features from open end aerator design at air velocity of 2.6 m/s.

These results indicate the reliability of the CFD method employed; the difference between CFD and experiment was lower than 5%. The preliminary grid independence was studied, an increase in the number of cells was found to have essentially no effect on bubble shape, size and velocity. Therefore, it was concluded that the simulations based on the mesh details herein provide a robust approach for studying free bubbling aeration.

3.2 Bubbly flow process

Firstly, the two configurations of aerator design are compared. Then in the following sections, hydrodynamics influence from channel gap and air flow rate are presented. Topics covered are principally hydrodynamics, including bubble features and shear stress, and aeration consumption. The choice of variables not explicitly investigate herein are based upon our previous studies, particularly Wang *et al* [28, 29].

The free bubbling process from two designs of aerator is shown in Fig. 5 (a). The bubbles continuously flow out from the pipe apertures, and being impeded by the base of the membranes, there is build up in the zone under the membrane. The bubbles were in a

dynamic status of merging and breakup, a number of fine bubbles formed as shown in Fig. 5 (a). Given that the only outlet is between the plates, the bubbles are squeezed into the channels between membranes where they flow upwards and induce shear stress on the surface of the membranes.

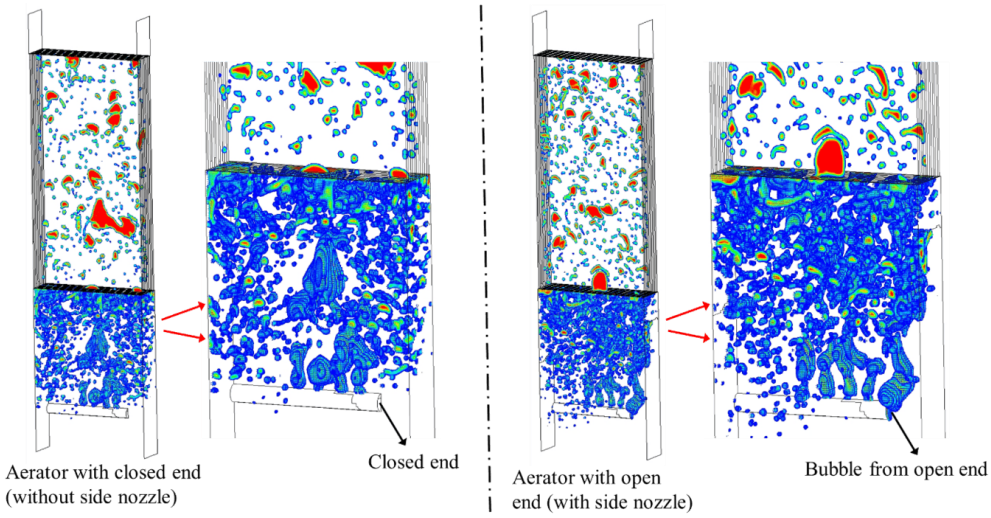

(a)

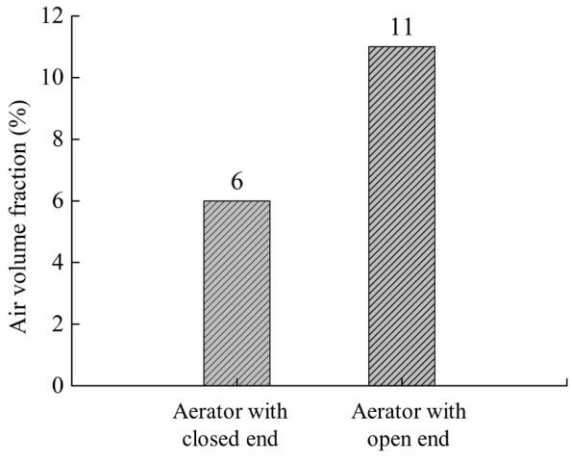

(b)

Fig. 5 (a) Comparison of the two configurations for the free bubbling process with inlet air speed of 2.6 m/s; (b) Fraction of air in the zone under the membrane plates for the two types of aerator.

The above results are due to the difference in the structure of the aerators; all other conditions such as the aeration rate of 2.6 m/s, membrane size of 448mm×245mm×6mm (L×W×T), and channel gap of 5 mm were the same. The presence of a side nozzle generated larger bubbles even though the air supply was the same. This led to a greater air fraction in the zone under the membranes – Fig. 5 (b). Although the air flow rate is the same the new design leads to improved hydrodynamic effects as detailed below.

3.3 Hydrodynamics effects

The hydrodynamic effect from different configurations of aerator was studied. Fig. 6 shows the CFD results for the two configurations of aerator with fine bubbles distribution in 6 channels. For configuration 1 one finds that in channels 1 and 2, which are positioned over the aerator, some bubbles are around 20 mm but a great portion of bubbles are extremely small in size at 1 ~ 3 mm. As for channel 3 and 4 there is a relative shift towards larger bubbles but most are still fine bubbles. Bubble size were much larger and around 80 mm maximum in channel 5 and 6.

For configuration 2, in which the aerator had a side nozzle in the pipe end, the bubble distribution among 6 channels was different from that of configuration 1. Fig. 6, shows that in channels 1, 4, 5 and 6, most parts of the membrane will experience the passage of large-sized bubbles of around 50 mm. Whilst for channel 2 and 3, there are fine bubbles with typical size of 4 mm and several bubbles around 25 mm.

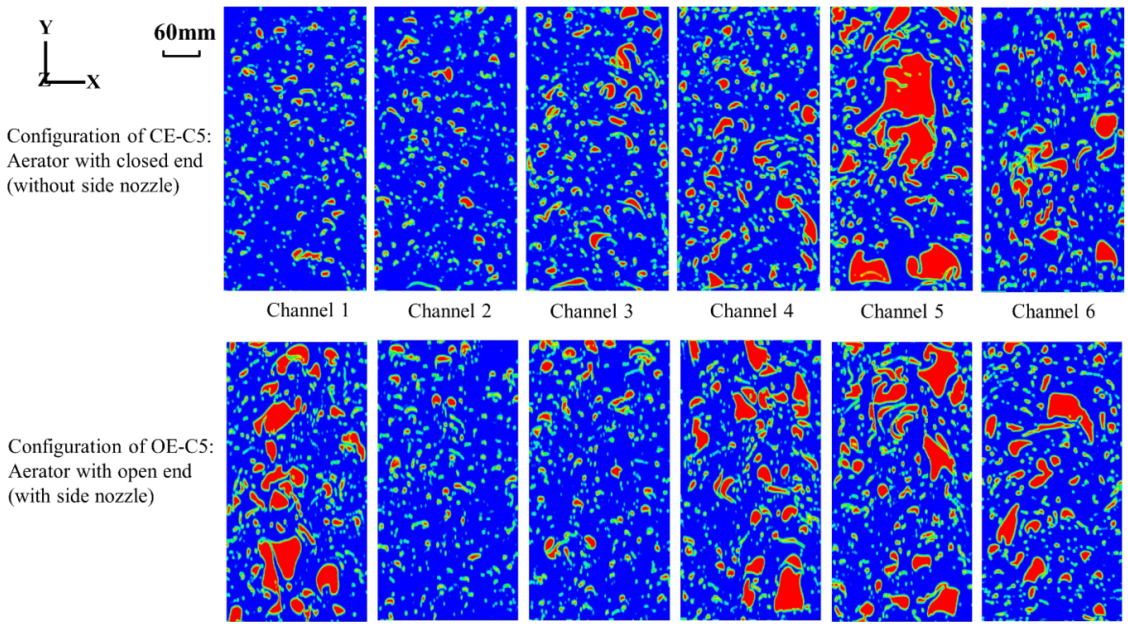

Fig. 6 Distribution of bubbles in six channels for both aerator configurations from CFD simulation.

Owing to its open end, configuration 2 generated a greater number of large bubbles and this in turn resulted in three more channels having bubbles of a larger size. Whilst the bubble in channel 5 of configuration 1 was much larger than those of other channels, there was great uniformity across the six channels with configuration 2. Shear stress induced by the bubbly flow was analyzed since this could directly influence the fouling propensity and be pivotal in deciding whether the innovative design amounts to a breakthrough.

Surface shear for all 6 channels for the two configurations are compared in Fig. 7 (a). For configuration 2, relatively high shear values across most membrane walls (i.e. red color represents shear stress $\geq$ 3 Pa) are found. In contrast the other configuration had one channel with high values of shear stress but most channels would only experience transient shear stresses of between 1-1.5 Pa. Fig. 7 (b) shows the detailed information indicating that configuration 2 will provide more effective hydrodynamics on fouling control [27, 28]. This figure indicates that the novel design is a significant breakthrough.

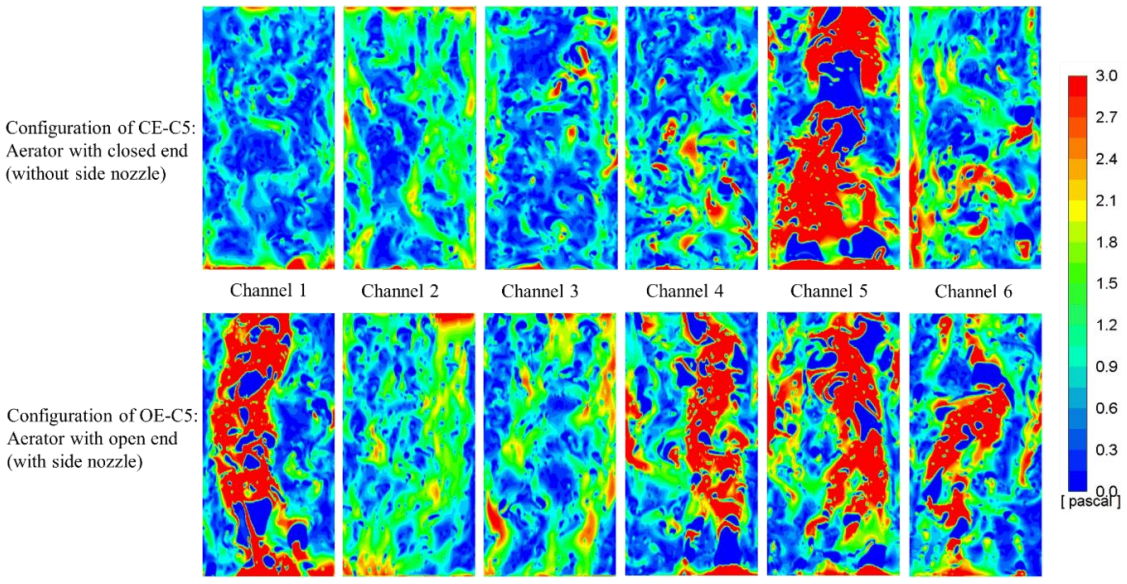

(a)

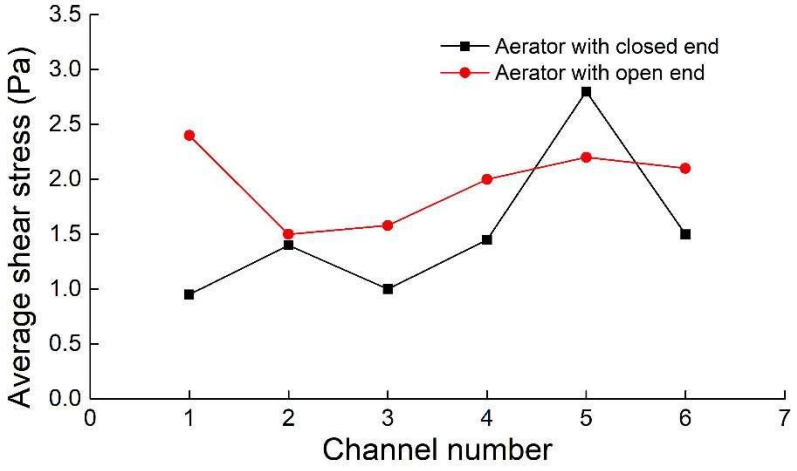

(b)

Fig. 7 (a) Wall shear stress distribution in all channels. (b) Comparison of average wall shear stress in all channels.

Fig. 8 (a) shows a side view illustrating the directions of flow. It indicates that the liquid flow in channels 1, 4, 5 and 6 is upwards and that in channels 2 and 3 is downwards.

This generates a liquid flow loop. Fig. 8 (b) shows that the downwards flow in channel 2. Such dominate flow impedes the ingress of large-sized bubbles. Overall this configuration has two channels with downwards liquid flow and four with upflow which generates stable and strong liquid circulation. In contrast the liquid flow patterns for the other configurations are weak.

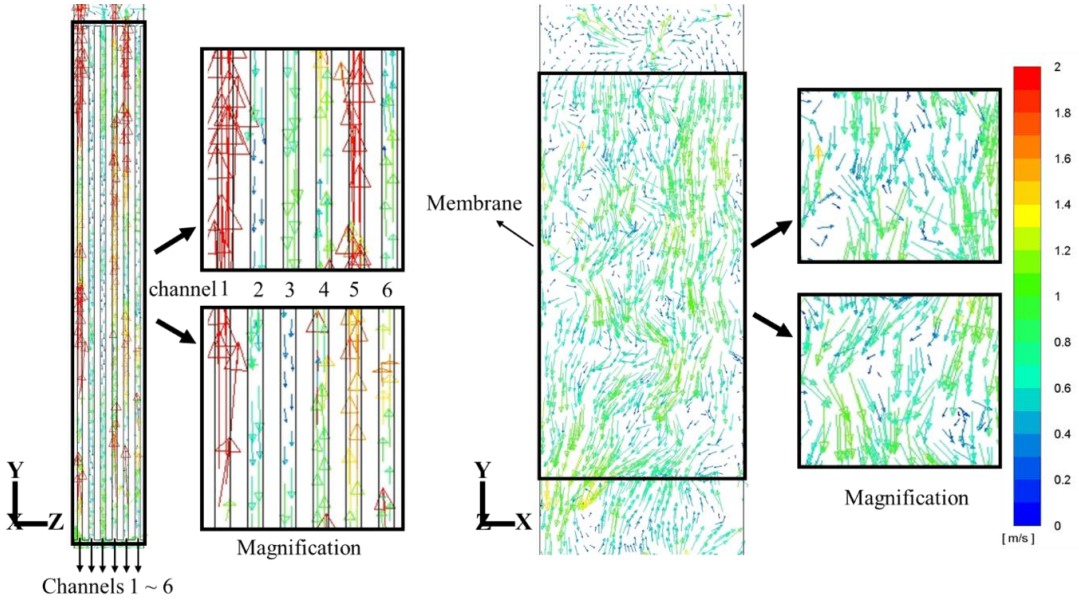

(a) from side view direction (b) from front view direction

Fig. 8 Velocity vectors and its magnification from CFD simulation for modified aerator system with open end (a) among different channels of 1 ~ 6; (b) for channel 2 with a dominant downwards flow.

To optimize the application of our innovative aerator (i.e. configuration 2) in the commercial mini type FSMBR system, two additional parameters were examined, namely the channel gap and the variation of air velocity. Additionally, section 3.6 covers the application of the new design to a full height FSMBR (i.e. 1800 mm).

3.4 Variation of Channel Gap

Based on this modified structure of aerator with an open end, the channel gap (space between two membranes) was varied from 3.5 mm to 7 mm. Fig. 9 provides a visual comparison of the influence of channel gap. For gaps between 3.5 mm to 5 mm, there was a similar distribution of bubbles among different channels. For all channel gap simulations, the bubbles in channel 1 were of somewhat larger size than those in other channels because the position of channel 1 is exactly above the aeration apertures, The average bubble size was 70 mm in channel 1, with maximum of 90 mm at gap of 4.5 mm. Whilst for the other 5 channels, the channels 2 and 3 had mainly the smaller bubbles of 1 ~ 3 mm, with few bubbles around 20 mm whilst the other three channels had somewhat larger sized bubbles. This variation in gas voidage will induce a beneficial flow loop of liquid as mentioned in Section 3.2.

The hydrodynamic effect due to bubbly flow depends on the gap interval because the gap influences the degree of resistance to liquid circulation. With a relatively small gap such as 3.5 mm, simulations indicated that weak localized upward flow might be expected in channel 5 (with relatively large bubbles of up to *circa* 60 mm with mostly fine bubbles in channels 4 and 6 (with few reaching *circa* 20 mm). However, as the gap increases to 4.5 mm the non-uniform distribution of bubbles among channel 4 to 6 was improved but the bubbles in channel 5 were still smaller than those in adjacent channels. When the gap was increased further to 5 mm, bubble distribution uniformity was improved, and for the four channels, channel 1 and channels 4 to 6, the bubble size was similar and around 50 mm.

For case (IV) in Fig. 9, with gap of 6 mm, the bubble size decreased in all the channels compared with those of case (III) because most of bubbles in the zone under the membranes

could flow directly into the channels. The outcome was that less channels had larger bubbles, which was not beneficial for the formation of the liquid flow loop. Moving to a gap of 7 mm, exacerbated the maldistribution and only the first channel had any large sized bubbles. Under these conditions, there was no dominant flow in either direction in most of the channels and consequently low shear stress as shown in Fig. 10.

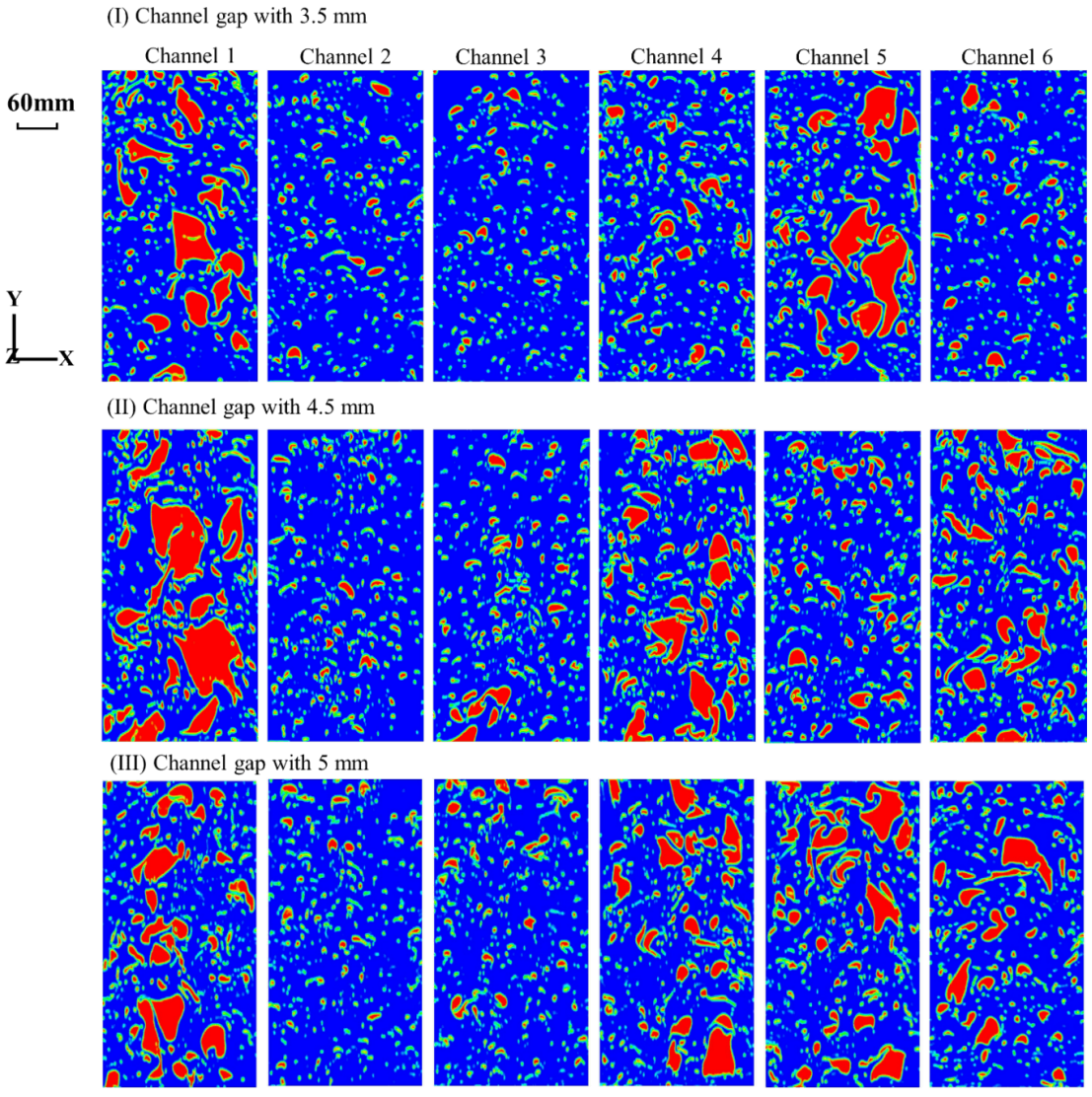

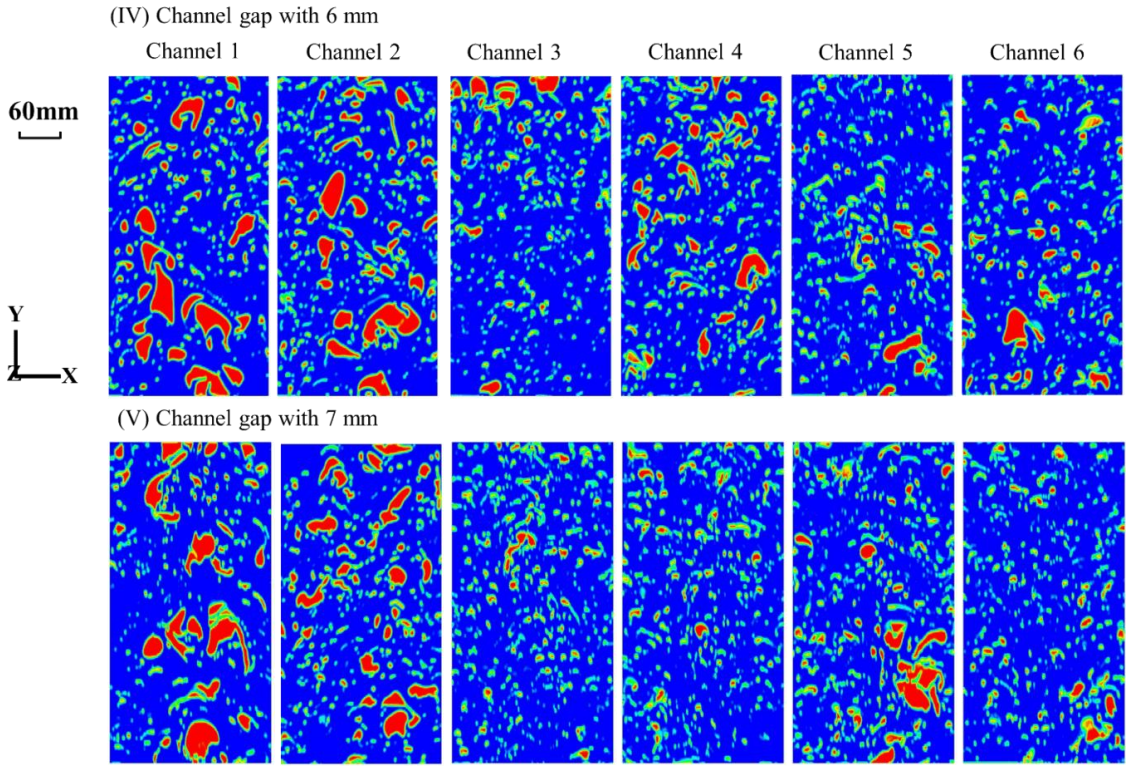

Fig. 9 Comparison of bubble distribution in channel gap from 3.5mm to 7 mm.

In Fig. 10, the induced shear stresses of the six channels were compared for various channel gaps. In all situations, in most regions of the membrane walls through the first channel, shear value was over 3 Pa. Through channels 2 to 6, the distribution of shear stress changed with the increase of channel gap. With a 3.5 mm channel gap, the shear stress of channel 5 was also high and most of its areas were over 3 Pa. For channel 4 and 6, there were few bubbles $\geq$ 20 mm, and no dominant flow direction. It was also found that channel 2 had a weaker flow and its shear stresses were lower with some areas only around 1.2 Pa. By contrast channel 3 had an obvious and intense dominant flow and had a more uniform distribution over the whole channel.

As the channel increased to be 4.5 mm and 5 mm, shear stress for channel 4 and 6 was enhanced, since the bubble size was larger. For channels 2 and 3, both cases (II) and (III) generate a dominant downwards flow and shear stress was uniform around 1.6 Pa. Shear stress in channel 5 at a gap 4.5 mm was lower than the values for gaps of 3.5 mm and 5 mm, but it was still modestly large in most of the areas at more than 1.5 Pa

Increasing the channel gap to 6 and 7 mm, led to low shear stress in some regions of channels 3 to 6; some portions had values less than 0.5 Pa in both cases and particularly low values with the larger gap. This was due to flow being dominated by that in channels 1 and 2. A summary which showed the mean shear stress for all six channels for all cases is given in Fig. 10 (b). In all cases, the first two channels had shear stresses greater than 2.3 Pa with the difference of in shear stress values being less than 1 Pa. Significant differences were observed in the other channels. With a channel gap of 5 mm (OE-C5), the shear stress of all six channels was more than 1.5 Pa and this size of gap provided both the most uniform and the highest mean value as illustrated in Fig. 10 (b). It will be recalled that the simulation was, due to symmetry, for half a system. So the results imply that in the entire system (both sides of center), one aerator should provide effective fouling control for twelve channels.

Examining the results either side of 5mm, it is seen that a gap interval of 4.5 mm (OE-C4.5), although it had smaller shear stress values than that of gap 5 mm, a good spatial distribution of shear stresses around 1.5 Pa was still evident which would imply that effective fouling control for all 12 channels would also be provided with this layout. In contrast to this, other gaps (i.e. OE-C3.5, OE-C6 and OE-C7) had some channels where the shear stress was less than 1.5Pa. Thus a channel gap between 4.5mm and 5mm is

recommended as this provides relatively uniform shear stress and sufficient hydrodynamic effect.

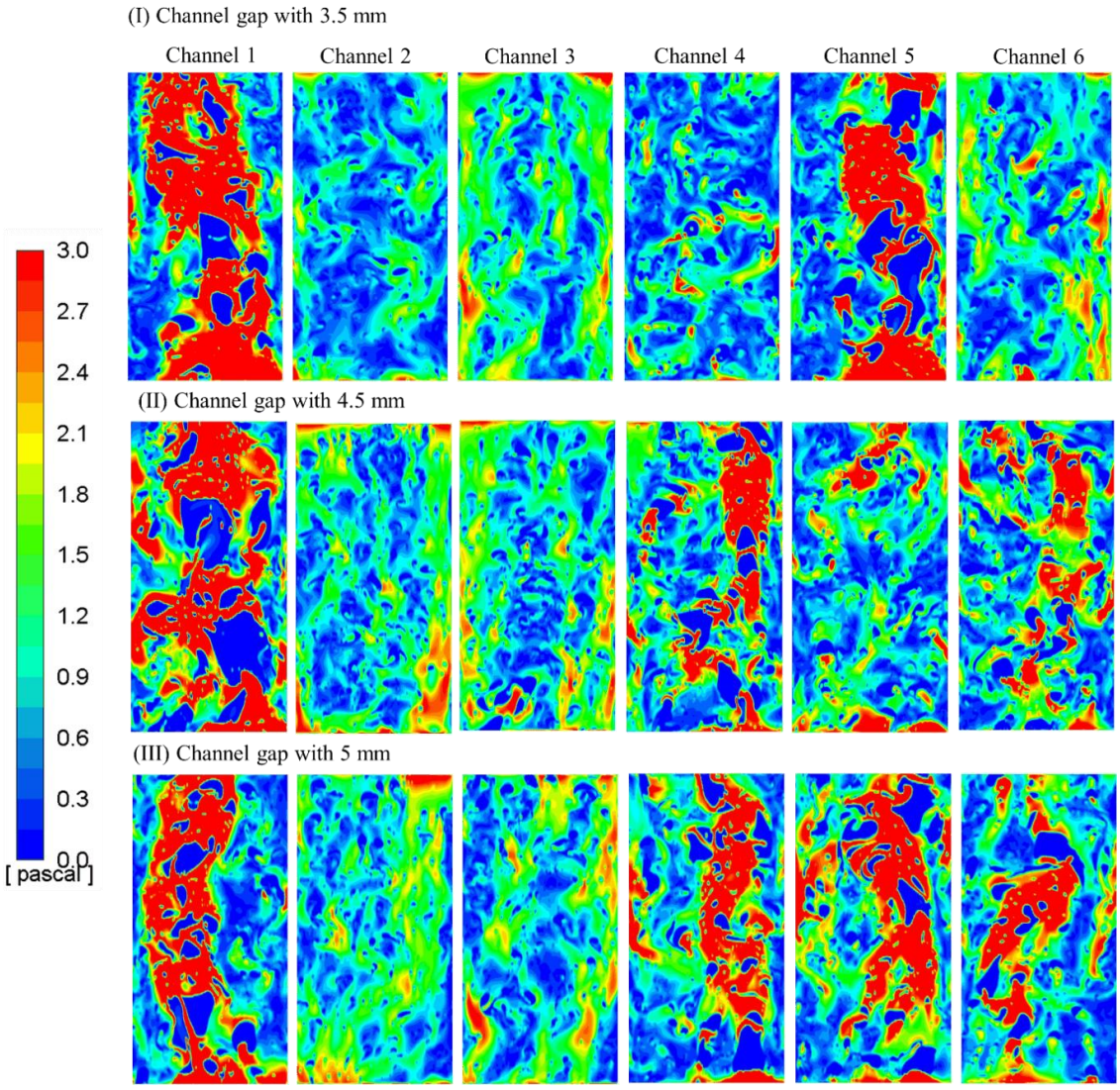

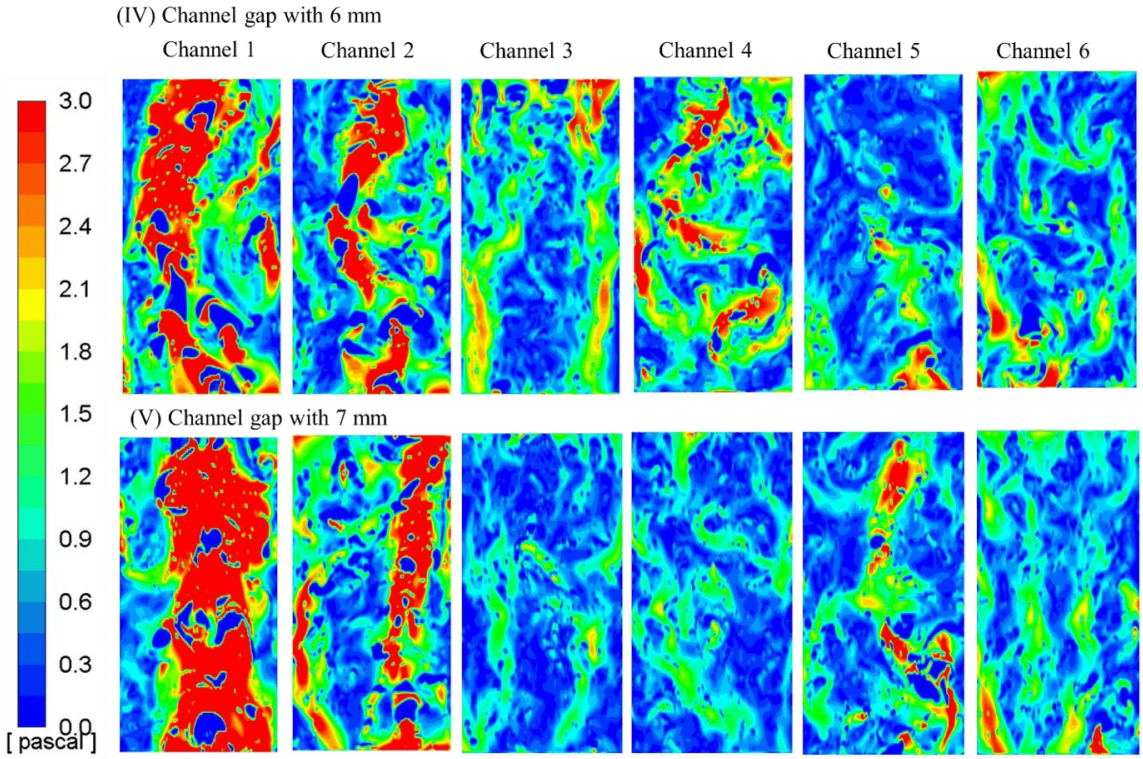

(a)

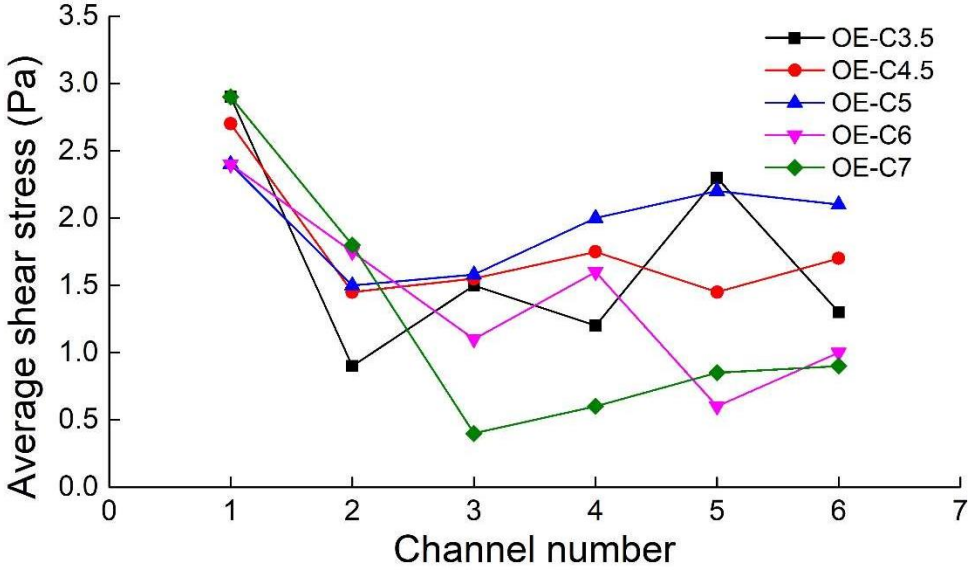

(b)

Fig. 10 Comparison of shear stress of 3.5 mm to 7mm different channel gap: (a) distribution of membrane surface shear stress; (b) shear stress average values.

3.5 Variation of air velocity

For industry, the aeration velocity is also a key parameter in the design of a mini FSMBR. For the same fixed conditions of membrane size (488mm×245mm×6mm (L×W×T)) and 5 mm channel gap, different air flow rates were investigated. This is expressed in terms of a pipeline air velocity at the inlet as illustrated in Fig. 2. Values were varied between 1 m/s and 3.7 m/s. Fig. 11 summarizes the effect of air velocity upon bubble distribution across the various channels. At a velocity of 1 m/s, bubbles *circa* 25 mm are confined to channels 1 and 2, with mostly fine bubbles in channel 3 to 6. As air velocity is increased to $\geq$ 2 m/s, large size bubble around 50 mm could be observed, which is beneficial for the formation of liquid circulation loops. The bubble size and distribution were similar as an air velocity of 2.6 m/s. At least three channels had larger sized bubble of around 50 mm, and other channels had fine bubbles. However further increases to air velocities to 3 m/s as well as 3.7 m/s creates maldistribution with lateral displacement. Shear stresses in all channels are plotted in Fig. 12 (a), whilst Fig. 12 (b) gives a comparison for the various values of air velocity.

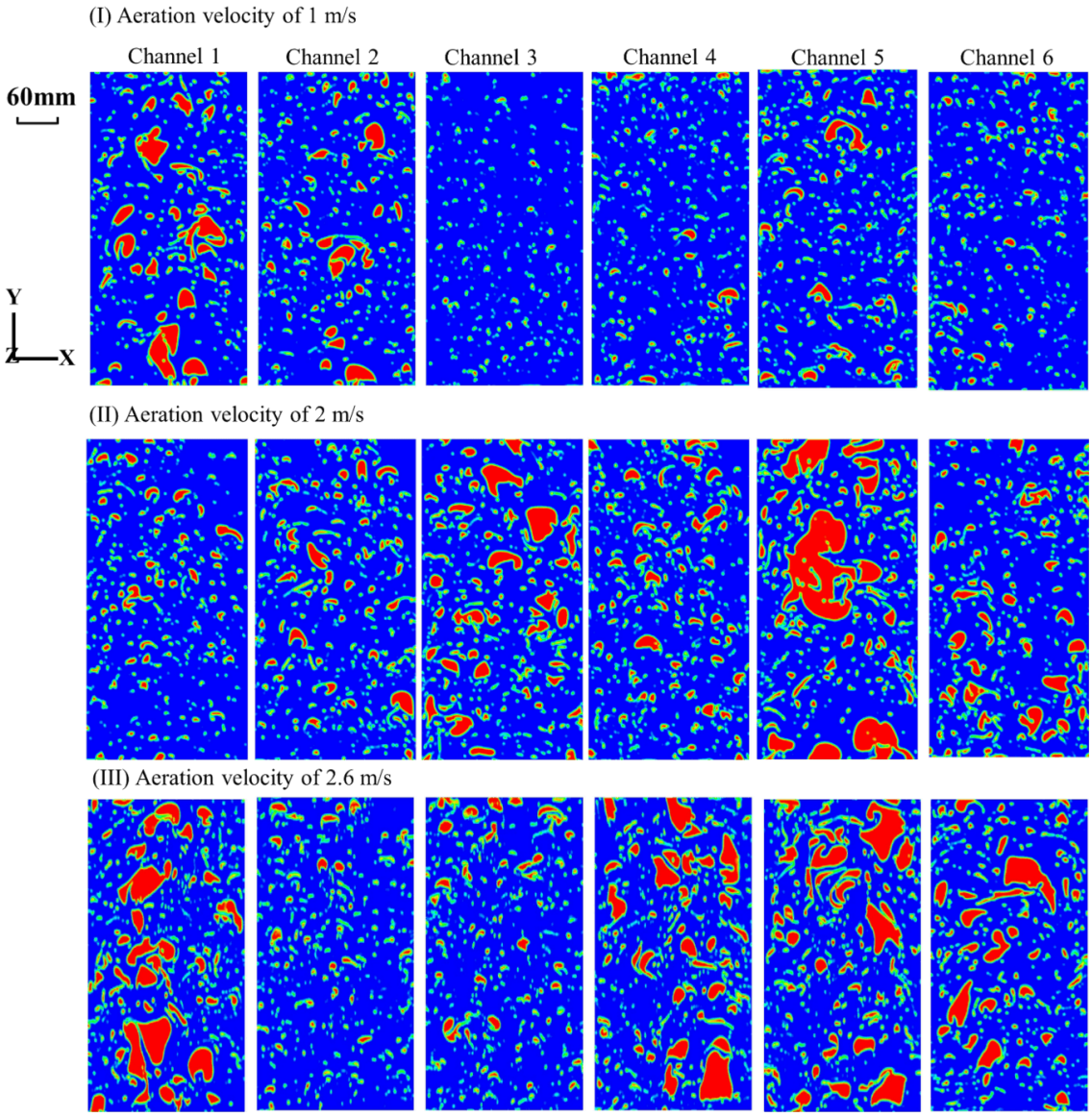
(I) Aeration velocity of 1 m/s
Channel 1
Channel 2
Channel 3
Channel 4
Channel 5
Channel 6
60mm
Y
Z
X
(II) Aeration velocity of 2 m/s
(III) Aeration velocity of 2.6 m/s

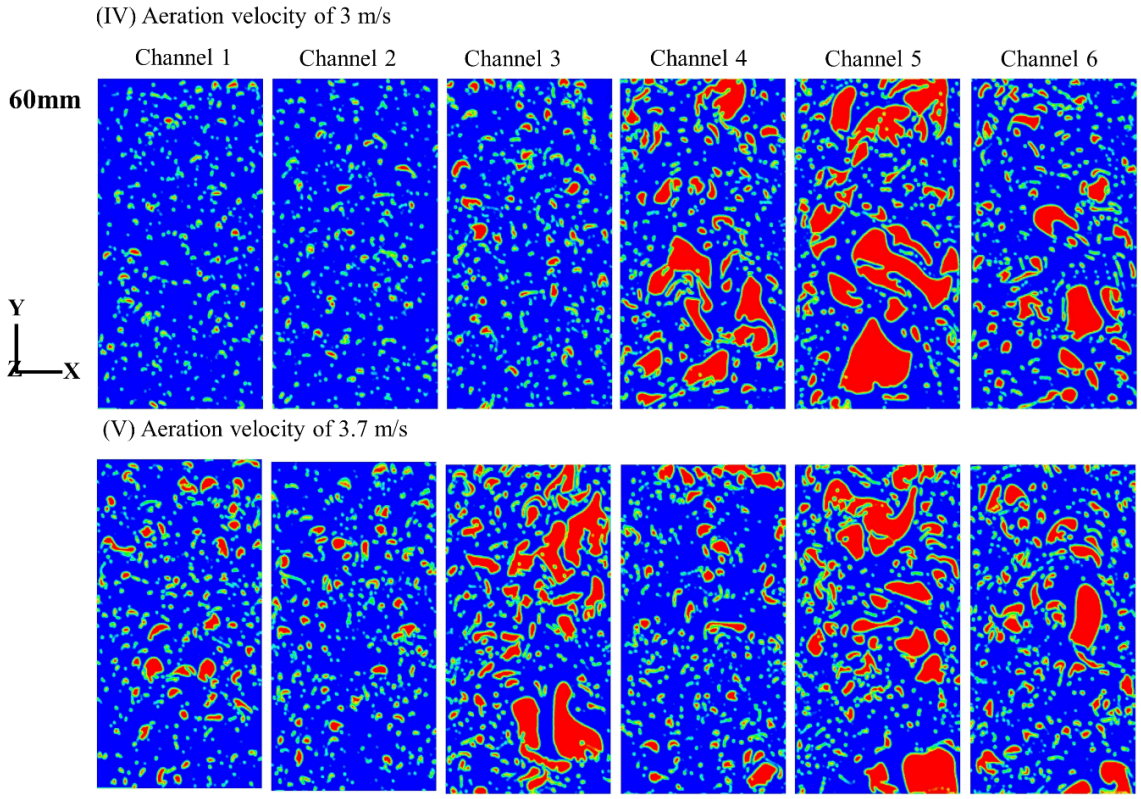

Fig. 11 Comparison of bubble distribution at different air velocity of 1 m/s to 3.7 m/s.

For some areas of the membrane surface in the first two channels, shear stresses generated by the bubbles for the lowest flowrate were over 3 Pa, and around 1 Pa in the channel 3, but in other three channels, for most regions it became only around 0.4 Pa. With air velocity increasing to more than 2 m/s, shear stress was more than 1.2 Pa for most areas in all channels. For 2 m/s all the channels had similar values, as displayed in Fig. 12 (b), except channel 5 which had the highest average value at 2.5 Pa. As shown in Fig. 12 (b) there was further enhancement in both uniformity and average values as air speed increased to 2.6 m/s whereas at higher velocities there was a lack of similarity from channel to channel. As a degree of uniformity in shear stress distribution among different channels is desirable an aeration speed with 2.6 m/s has been deemed optimal.

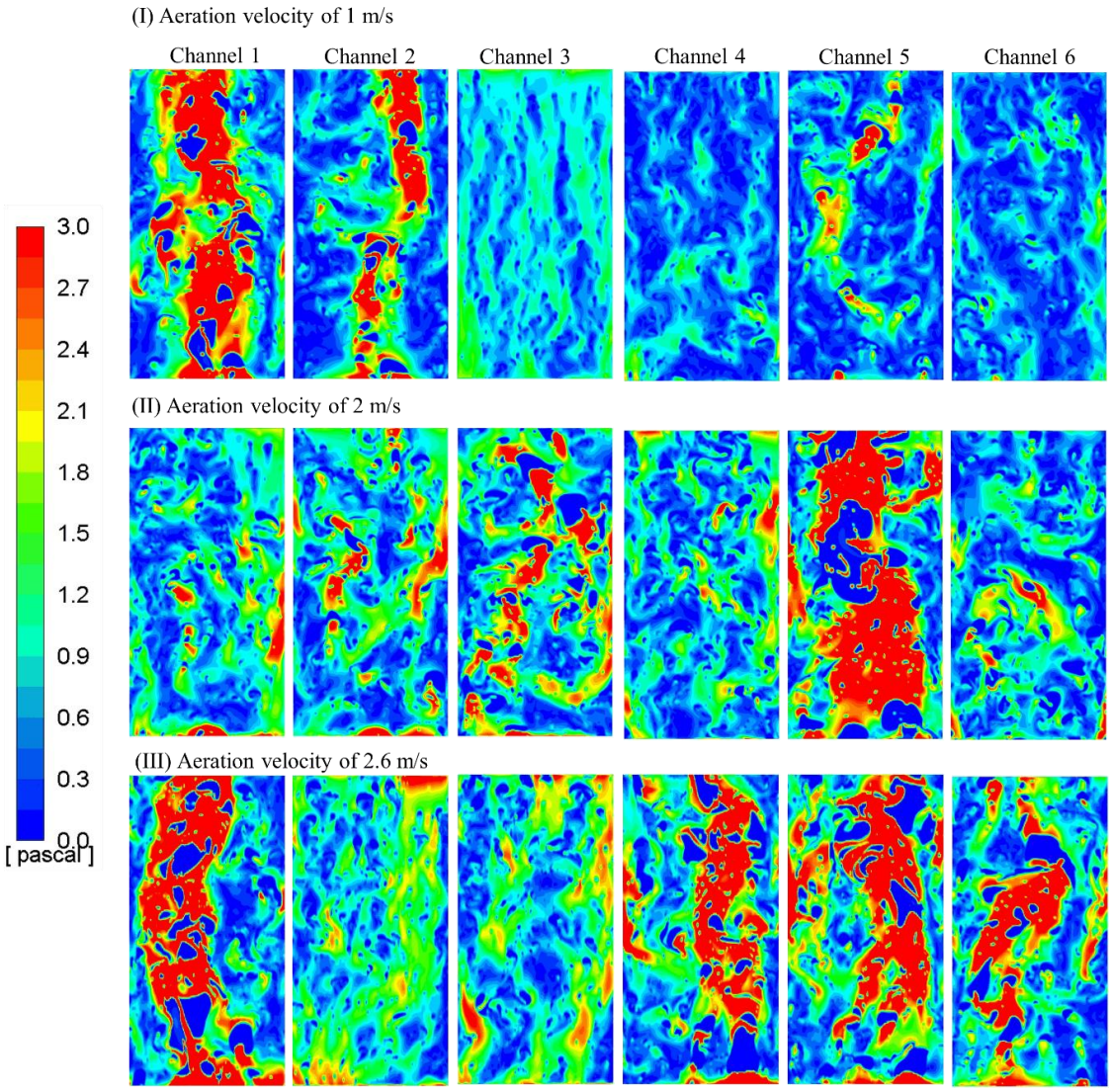
(I) Aeration velocity of 1 m/s
Channel 1
Channel 2
Channel 3
Channel 4
Channel 5
Channel 6
3.0
2.7
2.4
2.1
1.8
1.5
1.2
0.9
0.6
0.3
0.0
[pascal]
(II) Aeration velocity of 2 m/s
(III) Aeration velocity of 2.6 m/s

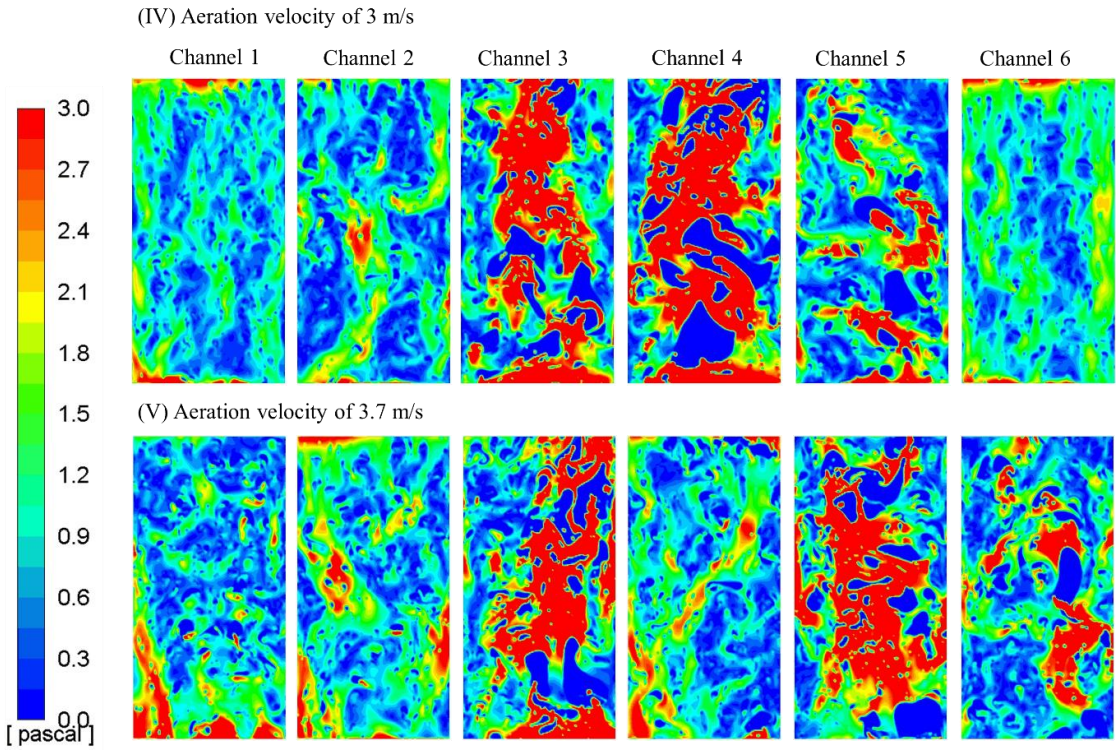

(a)

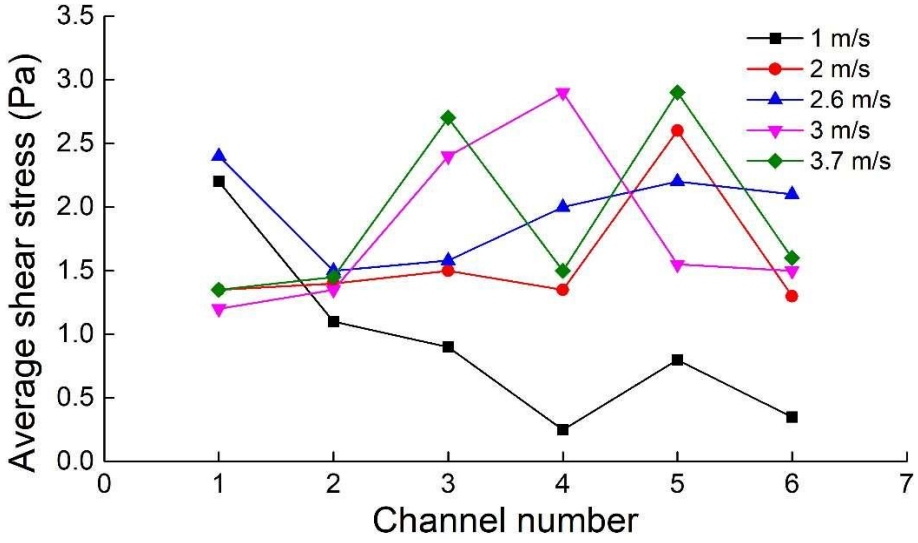

(b)

Fig. 12 Shear stress comparison under various aeration speeds between 1 m/s and 3.7 m/s: (a) distribution of wall shear stress values; (b) average values.

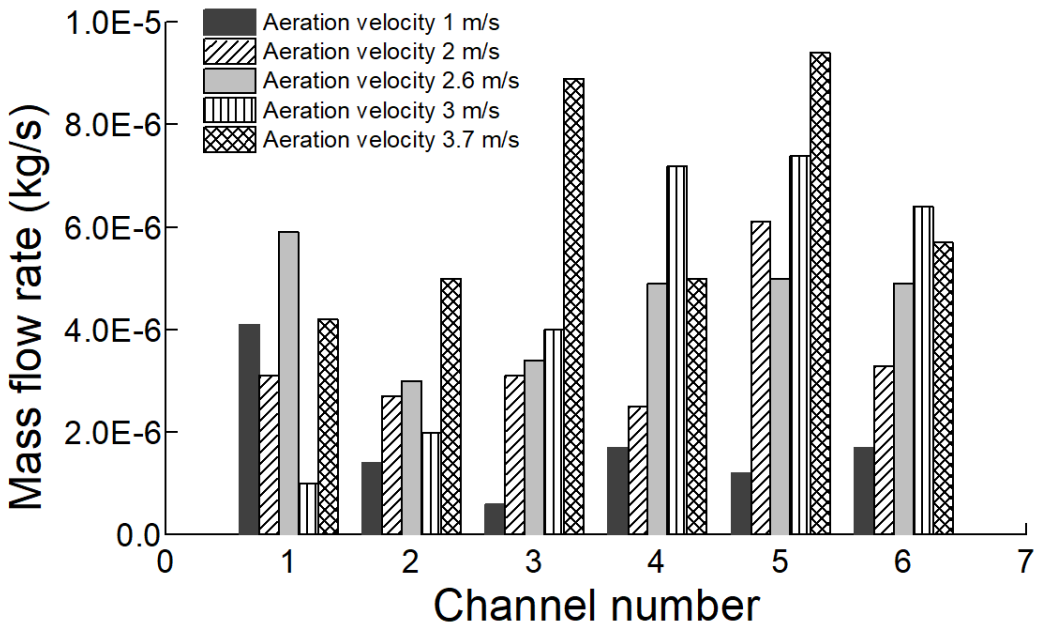

Fig. 13 Time-averaged mass flow of air into different channels under 5 aeration velocity (from 1 m/s to 3.7 m/s).

The membrane wall shear stress is partially influenced by the total flux of air bubbles into channels. Further, the air flux into different channels is directly dependent on the aeration velocity. The mass flow rate of air into all the channels for 5 aeration speeds are plot in Fig. 13. It shows that at the lowest velocity of 1 m/s all of the channels, with the exception of the first channel, had very small air flow rates. As the aeration velocity increases to 2 and 2.6 m/s, the air mass flow rates and uniformity increases. The case of 2.6 m/s presents the most uniform air mass flow rate distribution with values in each channel above 3.5×10^{-6} kg/s. At higher aeration velocities, such as 3 m/s and above, the air flow rates across the channels are very variable; whilst some channels reach high values (9×10^{-6} kg/s), some channels have very small values (1×10^{-6} kg/s). Thus for good uniformity there is an optimal value which is around 2.6 m/s.

3.6 Full-scale FSMBR with 1800 mm membrane height

The possibility of using the new innovative aerator design that had been developed for the mini type of FSMBR, in a large-scale one with membrane dimensions of 1800mm×490mm×6mm (L×W×T) was investigated. Air inlet velocity was 2.6 m/s. Its output in Figs. 14 and 15 can be compared with the relevant parts of Figs. 11 and 12. The increased height has led to a reduction in uniformity but the average shear stresses in all channels were over 1.5 Pa. A three-fold distribution is found. In channels 4 and 5 it is over 3 Pa and in channels 1 and 2 it is more than 1.5 Pa, whilst in channels 3 and 6 there is intense downwards flow of liquid and the shear stress in most regions is over 1.5 Pa.

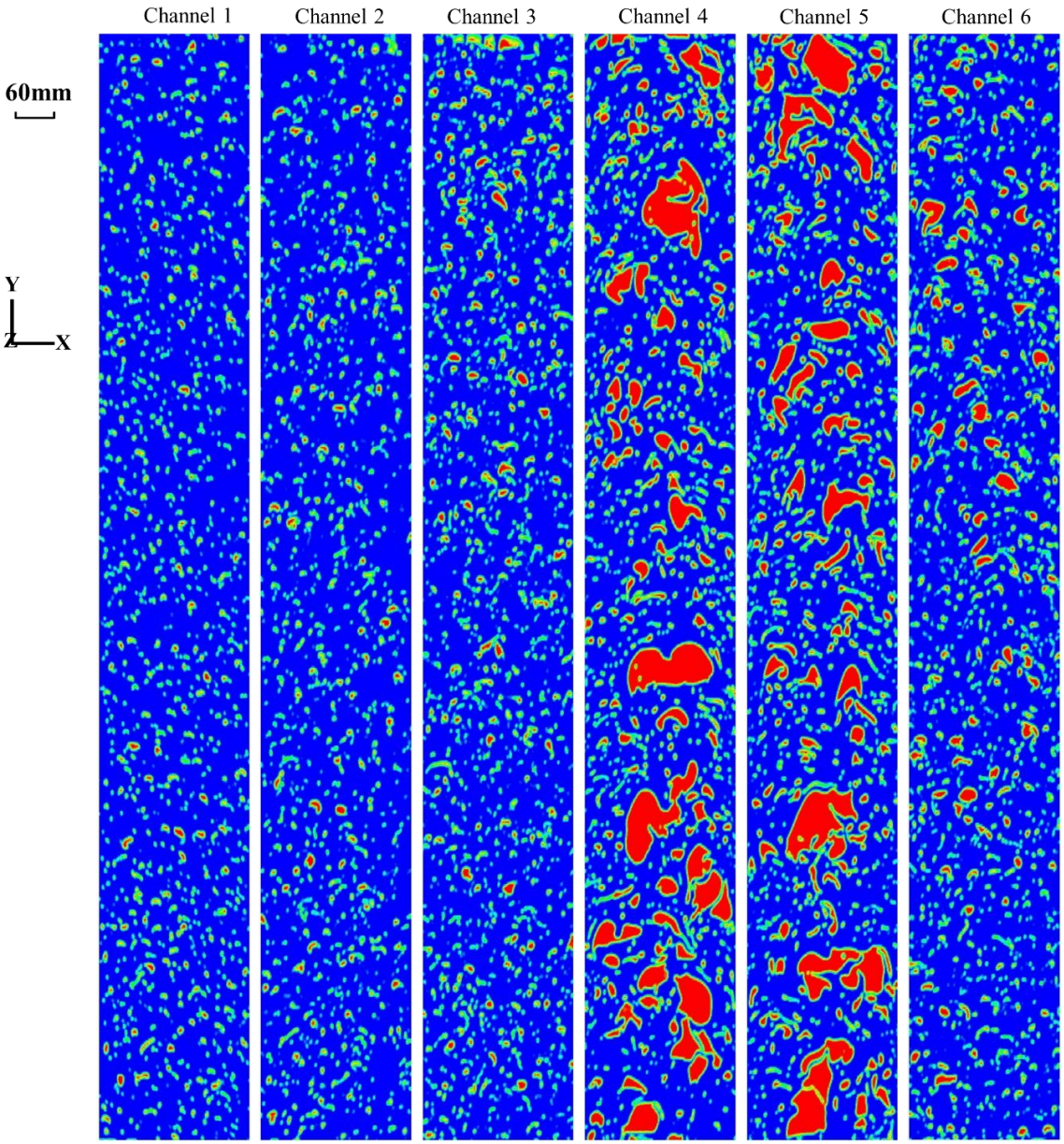

Fig. 14 Bubble distribution comparison for membrane height of 1800 mm with inlet air speed of 2.6 m/s.

Bubble distribution for a plate height of 1800 mm is given in Fig. 14; the large bubbles in channels 5 and 6 create intense upflow in these channels and downflow in the adjacent channels. The resultant shear stresses are presented in Fig. 15. Its average values are

displayed in Fig. 15 (b). These results are for the air speed of 2.6 m/s. Future work with this greater height of 1800 mm will investigate whether a slight reduction in air velocity is desirable. However the inlet velocity of 2.6 m/s did give satisfactory coverage of all channels as judged by the fact that all shear stresses are greater than 1.5 Pa.

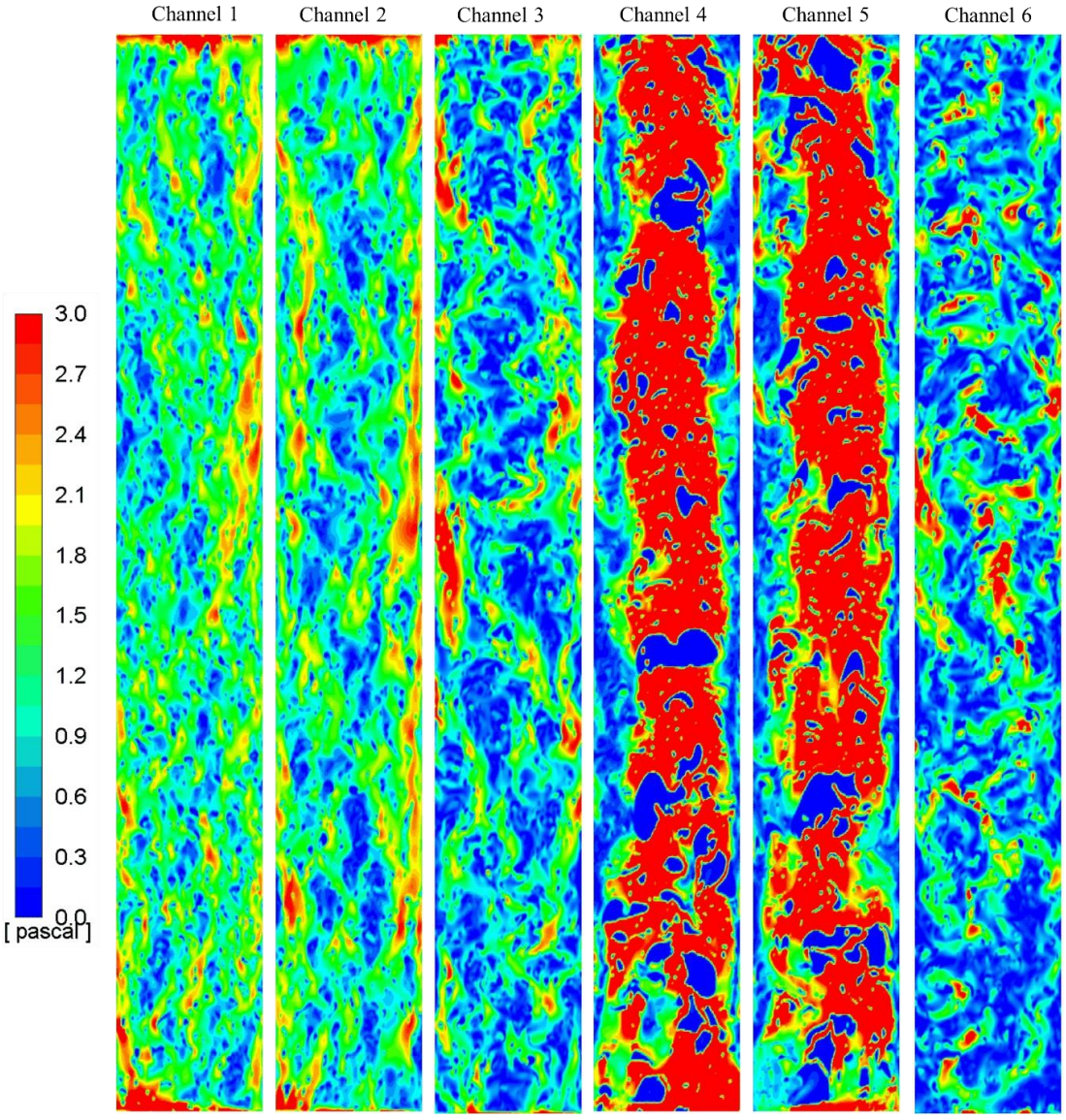

(a)

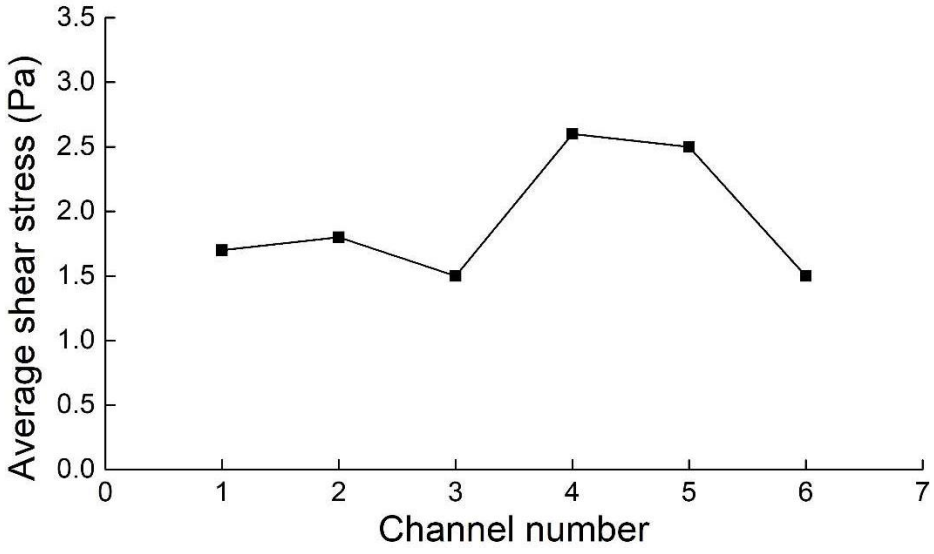

(b)

Fig. 15 Shear stress among 6 channels for large-scale FSMBR of 1800 mm height at air velocity of 2.6 m/s: (a) distribution of shear stress; (b) average values of shear stresses.

3.7 Air Consumption

From above results, the aeration rate per sheet membrane and the total aeration rate for the FSMBR with 100 membrane sheets can be estimated. Based on the resultant shear stresses in Figs. 10 (b), 12 (b) and Fig. 15 (b), and by considering the number of channels with average shear stress >1.5Pa that are effectively covered by one aerator, the air consumption has been calculated for all conditions. Where the simulations have indicated values of less than 1.5 Pa the air consumption was increased pro rata because more aerators would need to be deployed e.g. if four out of six channels were covered the factor was 1.5. Where a pro rata factor has been applied these values are rough estimates, whereas for the cases where all six channels were covered the calculations are accurate. The results are given in Table 4.

Table 4 Comparison of air consumption in free bubbling MBRs

FSMBR with channel gap 5 mm, including 100 sheets of membranes sized 1800mm×490mm×6mm (L×W×T)

Air Velocity (m/s)	Number of effective channel coverage	Air flow rate (L/min·sheet)	Total air consumption (L/min)	SAD_m, $Nm^3m^{-2}h^{-1}$	Percentage of consumption saved (%)
2.6	6	8.16	816	0.28	46
Traditional industrial usage	--	15	1500	0.51	--

FSMBR with channel gap 5 mm, including 100 sheets of membranes in the size of 448mm×245mm×6mm (L×W×T)

Air Velocity (m/s)	Number of effective channel coverage	Air flow rate (L/min·sheet)	Total air consumption (L/min)	SAD_m, $Nm^3m^{-2}h^{-1}$	Percentage of consumption saved (%)
1	1	9.42	942*	2.36	n/a
2	3	6.28	628*	1.57	23
2.6	6	4.08	408	1.02	50
3	4	7.06	706*	1.77	13
3.7	4	8.71	871*	2.18	0
Traditional design with closed end	3	8.16	815	2.05	--

* These are estimates based upon pro rata calculation as explained in the text.

The minimum aeration rate of 4.08 L/min•sheet has been determined for a channel gap of 5 mm coupled with an air velocity of 2.6 m/s. This value was compared with that of the

traditional design of aerator with closed end. Savings ranged up to 50%, which indicates that for the free bubbling process, the innovative aerator can reduce air consumption whilst giving effective amelioration of fouling. The optimized parameters for this modified design of free bubbly flow is determined to be a channel gap of 5mm coupled with aeration speed of 2.6 m/s as it induces the most uniform distribution of high shear stress.

Our new innovative design of aerator was not only coupled with the mini type of FSMBR. Simulations were also made with a large-scale FSMBR with standard plates of 1800mm×490mm×6 mm (L×W×T). The conditions that were optimal for the mini FSMBR, namely a channel gap of 5 mm and air velocity of 2.6 m/s, were found to be suitable for the larger system. Importantly these conditions correspond to an air flow rate of 8.16 L/min·sheet and a SAD_m of 0.28 $Nm^3m^{-2}h^{-1}$, which is close to half of the normal usage in industry of 15 L/min·sheet and a corresponding SAD_m value of 0.51 $Nm^3m^{-2}h^{-1}$. Therefore the expectation is that a beneficial saving of *circa* 46% can be made.

4. Concluding Remarks

An innovative aerator design for a free bubbling process was developed and optimized *in silico* for a mini FSMBR. Simulations indicate that an aerator with an additional side nozzle (simply an open end) can be optimized to produce beneficial hydrodynamics. The code used for the simulations has previously been validated experimentally as indicated above and additional comparisons with experiments are given herein. The bubbly flow from a single branch aerator can cover 12 channels. Shear stress development for different conditions of channel gap and aeration velocity were compared. It can be determined that a gap between 4.5 mm to 5 mm should induce a high shear stress in all channels with more

intense upwards flow in two-thirds of the channels, and a correspondingly dominant downward flow in the other channels. An aerator velocity of 2.6 m/s optimizes the bubble distribution and shear stress generation.

Although this open-end aerator design was designed for mini type of FSMBR, it is also applicable for use in a large-scale FSMBR with plate dimensions of 1800mm×490mm×6mm (L×W×T). Intense and dominant bubbly flow were observed in each channel, wherein a combination of upwards and downwards flow results in globally high shear stress. In general, the results demonstrated that the design conditions should be a 5 mm channel gap and a 2.6 m/s aeration velocity. Moreover, the total aeration consumption was estimated to give a saving of up to 50% compared with that of a traditional design based on closed-end aerators. For a process where air compression is the dominant operating cost these are highly significant findings.

Acknowledgements

This work was supported by grants from the National Key R&D Program of China (2018YFC1903205); Ministry of Science and Technology, the Bureau of Frontier Sciences and Education (QYZDB-SSW-DQC044); the Bureau of International Cooperation (132C35KYSB20160018); the Chinese Academy of Sciences and the Joint Project between CAS-CSIRO (132C35KYSB20170051); FJIRSM&IUE Joint Research Fund (No. RHZX-2019-002); the Fundamental Research Funds for the Central Universities, Nankai University (63201128). The authors would like to thank the grant of “antifouling membranes and slug bubbling flat sheet membrane bioreactors for the next generation wastewater treatment” and Oxiamembrane Co.Ltd for technical support. RWF

acknowledges the support provided by an APEX project on water reuse that has been supported by the Royal Society in partnership with the British Academy and the Royal Academy of Engineering together with generous support from the Leverhulme Trust. The authors also thank Mr. Xingbiao Chen and Dr. Olusegun Abass for their help and industrial perspective.

References

[1] Z.F. Cui, Experimental investigation on enhancement of crossflow ultrafiltration with air sparging, Effective Membrane Processes—New Perspectives., Mechanical Engineering Publications Ltd, London, (1993) 237–245.
[2] R.W. Field, K. Zhang, Z. Cui, B.K.J.D. Hwang, W. Treatment, Flat sheet MBRs: analysis of TMP rise and surface mass transfer coefficient, 35 (2011) 82-91.
[3] Z.F. Cui, S. Chang, A.G. Fane, The use of gas bubbling to enhance membrane processes, Journal of Membrane Science, 221 (2003) 1-35.
[4] P. Le-Clech, V. Chen, T.A.G. Fane, Fouling in membrane bioreactors used in wastewater treatment, Journal of Membrane Science, 284 (2006) 17-53.
[5] F. Zamani, H.J. Tanudjaja, E. Akhondi, W.B. Krantz, A.G. Fane, J.W. Chew, Flow-field mitigation of membrane fouling (FMMF) via manipulation of the convective flow in cross-flow membrane applications, Journal of Membrane Science, 526 (2017) 377-386.
[6] A.Y. Kirschner, Y.-H. Cheng, D.R. Paul, R.W. Field, B.D. Freeman, Fouling mechanisms in constant flux crossflow ultrafiltration, Journal of Membrane Science, 574 (2019) 65-75.
[7] T. Sano, Y. Koga, H. Ito, L.V. Duc, T. Hama, Y. Kawagoshi, Effects of structural vulnerability of flat-sheet membranes on fouling development in continuous submerged membrane bioreactors, Bioresource Technology, 304 (2020) 123015.
[8] Y. Wibisono, E.R. Cornelissen, A.J.B. Kemperman, W.G.J. van der Meer, K. Nijmeijer, Two-phase flow in membrane processes: A technology with a future, Journal of Membrane Science, 453 (2014) 566-602.
[9] R.W. Field, J.J. Wu, 2.1 Fundamentals of Crossflow Microfiltration, in: E. Drioli, L. Giorno, E. Fontananova (Eds.) Comprehensive Membrane Science and Engineering (Second Edition), Elsevier, Oxford, 2017, pp. 1-14.
[10] L. Fortunato, L. Ranieri, V. Naddeo, T. Leiknes, Fouling control in a gravity-driven membrane (GDM) bioreactor treating primary wastewater by using relaxation and/or air scouring, Journal of Membrane Science, 610 (2020) 118261.
[11] H. Liu, J. Gu, S. Wang, M. Zhang, Y. Liu, Performance, membrane fouling control and cost analysis of an integrated anaerobic fixed-film MBR and reverse osmosis process for municipal wastewater reclamation to NEWater-like product water, Journal of Membrane Science, 593 (2020) 117442.

[12] P. Krzeminski, J.A. Gil, A.F. Nieuwenhuijzen, J. van der Graaf, Flat sheet or hollow fibre — comparison of full-scale membrane bio-reactor configurations, Desalination and Water Treatment, 42 (2012) 100-106.
[13] M. Dalmau, H. Monclús, S. Gabarrón, I. Rodriguez-Roda, J. Comas, Towards integrated operation of membrane bioreactors: Effects of aeration on biological and filtration performance, Bioresource Technology, 171 (2014) 103-112.
[14] K. Essemiani, G. Ducom, C. Cabassud, A. Liné, Spherical cap bubbles in a flat sheet nanofiltration module: experiments and numerical simulation, Chemical Engineering Science, 56 (2001) 6321-6327.
[15] A.A. Kulkarni, J.B. Joshi, Bubble formation and bubble rise velocity in gas-liquid systems: A review, Industrial and Engineering Chemistry Research, 44 (2005) 5873-5931.
[16] P. Wei, K. Zhang, W. Gao, L. Kong, R. Field, CFD modeling of hydrodynamic characteristics of slug bubble flow in a flat sheet membrane bioreactor, Journal of Membrane Science, 445 (2013) 15-24.
[17] X. Du, X. Liu, Y. Wang, E. Radaei, B. Lian, G. Leslie, G. Li, H. Liang, Particle deposition on flat sheet membranes under bubbly and slug flow aeration in coagulation-microfiltration process: Effects of particle characteristic and shear stress, Journal of Membrane Science, 541 (2017) 668-676.
[18] M. Yang, D. Yu, M. Liu, L. Zheng, X. Zheng, Y. Wei, F. Wang, Y. Fan, Optimization of MBR hydrodynamics for cake layer fouling control through CFD simulation and RSM design, Bioresource Technology, 227 (2017) 102-111.
[19] A. Pinilla, J.C. Berrio, E. Guerrero, J.P. Valdés, D. Becerra, P. Pico, L. Vargas, S. Madsen, T.R. Bentzen, N. Ratkovich, CFD modelling of the hydrodynamics in a filtration unit with rotating membranes, Journal of Water Process Engineering, 36 (2020) 101368.
[20] M. Liu, M. Yang, M. Chen, D. Yu, J. Zheng, J. Chang, X. Wang, C. Ji, Y. Wei, Numerical optimization of membrane module design and operation for a full-scale submerged MBR by computational fluid dynamics, Bioresource Technology, 269 (2018) 300-308.
[21] E. Radaei, X. Liu, K.H. Tng, G. Merendino, F.J. Trujillo, P.R. Bérubé, G. Leslie, Numerical and experimental investigation of pulse bubble aeration with high packing density hollow-fibre MBRs, Water Research, 160 (2019) 60-69.
[22] K. Zhang, Z. Cui, R.W. Field, Effect of bubble size and frequency on mass transfer in flat sheet MBR, Journal of Membrane Science, 332 (2009) 30-37.
[23] K. Zhang, R.W. Field, Z. Cui, Measurement of the mass transfer coefficients in submerged flat sheet membrane systems., The conference of the European Membrane Society., (2006).
[24] K. Zhang, P. Wei, M. Yao, R.W. Field, Z. Cui, Effect of the bubbling regimes on the performance and energy cost of flat sheet MBRs, Desalination, 283 (2011) 221-226.
[25] Q. Wu, X. Yan, K. Xiao, J. Guan, T. Li, P. Liang, X. Huang, Optimization of membrane unit location in a full-scale membrane bioreactor using computational fluid dynamics, Bioresource Technology, 249 (2018) 402-409.
[26] X. Liu, Y. Wang, Y. Shi, Q. Li, P. Dai, J. Guan, T.D. Waite, G. Leslie, CFD modelling of uneven flows behaviour in flat-sheet membrane bioreactors: From bubble generation to shear stress distribution, Journal of Membrane Science, 570-571 (2019) 146-155.
[27] B. Wang, K. Zhang, R.W. Field, Novel aeration of a large-scale flat sheet MBR: A CFD and experimental investigation, AIChE Journal, 64 (2018) 2721-2736.

[28] B. Wang, K. Zhang, R.W. Field, Slug bubbling in flat sheet MBRs: Hydrodynamic optimization of membrane design variables through computational and experimental studies, Journal of Membrane Science, 548 (2018) 165-175.
[29] B. Wang, K. Zhang, R.W. Field, Optimization of aeration variables in a commercial large-scale flat-sheet MBR operated with slug bubbling, Journal of Membrane Science, 567 (2018) 181-190.
[30] B. Wang, K. Zhang, R. Field, Novel economical three‐stage slug bubbling process in a large‐scale flat‐sheet MBR of double deck configuration, AIChE Journal, 66 (2020).
[31] C.W. Hirt, B.D. Nichols, Volume of fluid (VOF) method for the dynamics of free boundaries, Journal of Computational Physics, 39 (1981) 201-225.
[32] J.U. Brackbill, D.B. Kothe, C. Zemach, A continuum method for modeling surface tension, Journal of Computational Physics, 100 (1992) 335-354.
[33] T.-H. Shih, W.W. Liou, A. Shabbir, Z. Yang, J. Zhu, A new k-ϵ eddy viscosity model for high reynolds number turbulent flows, Computers & Fluids, 24 (1995) 227-238.

[34] http://www.oxiamem.com